THE JOURNAL OF PHYSICAL CHEMISTRY Letters

pubs.acs.org/JPCL

Surfactant Self-Assembly in Cylindrical Silica Nanopores

Dirk Müter,[†] Taegyu Shin,[‡] Bruno Demé,[§] Peter Fratzl,[†] Oskar Paris,[∥] and Gerhard H. Findenegg*[,‡]

[†]Max-Planck-Institute of Colloids and Interfaces, Department of Biomaterials, Research Campus Golm, 14424 Potsdam, Germany, [‡]Institute of Chemistry, Stranski Laboratory, Sekretariat TC7, Technical University Berlin, Strasse des 17. Juni 124, 10623 Berlin, Germany, [§]Institute Laue-Langevin, 6, rue Jules Horowitz B.P. 156, 38042 Grenoble Cedex, France, and [∥]Institute of Physics, University of Leoben, Franz-Josef-Strasse 18, 8700 Leoben, Austria

ABSTRACT The aggregative adsorption of a nonionic surfactant ($C_{12}E_5$) in the cylindrical pores of SBA-15 ordered mesoporous silica (pore diameter 8 nm) was studied by small-angle neutron scattering (SANS). Scattering profiles obtained at contrast-matching conditions between the aqueous solvent and the silica matrix can be represented quantitatively by an analytical scattering function for the diffuse small-angle scattering superimposed with Bragg reflections from the pore lattice. These two contributions provide complementary information about the self-assembly of the surfactant in the pores: diffuse scattering indicates the formation of surfactant aggregates at preferred distances from each other, and analysis of the Bragg peaks shows that a layer of surfactant is formed at the pore walls. These findings suggest that adsorption of the surfactant starts by formation of discrete surface aggregates, which increase in number and later merge to interconnected patches as the plateau of the adsorption isotherm is approached.

SECTION Surfactants, Membranes

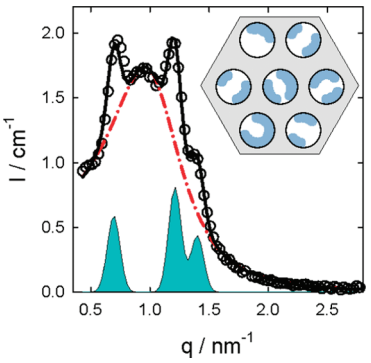

The adsorption of surfactants in narrow slits or channels plays a key role in diverse situations of technical relevance. For example, surfactants are strongly affecting the stability of colloids in aqueous media, and confinement-induced structural changes of adsorbed surfactant layers in a slit geometry have been studied both experimentally[1] and theoretically[2] to better understand the origin of this stabilization. Surfactant adsorption in nanoporous materials is of importance in membrane separation processes such as micellar-enhanced ultrafiltration.[3] It has also been recognized that the ability to control the morphologies of surfactant assemblies in nanoscale confinement can be relevant for applications in nanofluidics and nanomedical devices, including patterning the inner surface of nanochannels,[4] surfactant-modulated switching of molecular transport in nanometer-sized pores,[5] or the fabrication of asymmetric nanopores by track-etching techniques.[6]

Adsorption of surfactants onto hydrophilic surfaces represents a surface-aggregation process, driven by hydrophobic interactions similar to micellar aggregation in bulk solution.[7] Surface aggregation may lead either to surface micelles or extended bilayers, depending on the headgroup size and tail length of the surfactant and the density of adsorbing sites at the surface. Structural information about adsorbed surfactant layers at flat solid surfaces has been gained mainly by atomic force microscopy (AFM),[8] neutron reflectometry,[9] and grazing incidence small-angle neutron scattering (GISANS).[10] Curvature of the solid surface and confinement of the adsorption space in pores or channels may further affect the surface self-assembly of surfactants, but only few experimental studies so far have specifically addressed these effects.[11−13] In a recent SANS study[11] it was found that the nonionic surfactant *n*-dodecyl-penta(ethylene glycol) ($C_{12}E_5$) forms globular surface micelles on silica nanoparticles, although laterally homogeneous bilayers are reported for flat hydrophilic silica substrates.[8] This was attributed to the convex surface curvature of the silica nanoparticles, which prevents an effective packing of the surfactant molecules in a bilayer film. Confinement effects were reported to have a strong influence on the self-assembly of surfactant in pores when the pore radius approaches the width of a surfactant bilayer.[12,13] However, to our knowledge no direct structural studies have been performed until now for well-defined pore geometries. Two scenarios are envisaged when the surfactant concentration in the pores is gradually increased: either formation of surface micelles of distinct size and increasing number,[7] or nucleation and growth of a fragmented bilayer.[9] The aim of this work has been to find out which of these possibilities applies to the case of a nonionic surfactant in cylindrical pores with hydrophilic walls.

Here we report a SANS study of the self-assembled structures of the surfactant $C_{12}E_5$ in SBA-15 ordered mesoporous silica. SBA-15 particles constitute an array of cylindrical

Received Date: March 2, 2010
Accepted Date: April 9, 2010

DOI: 10.1021/jz100279y | *J. Phys. Chem. Lett.* **2010**, *1*, 1442–1446

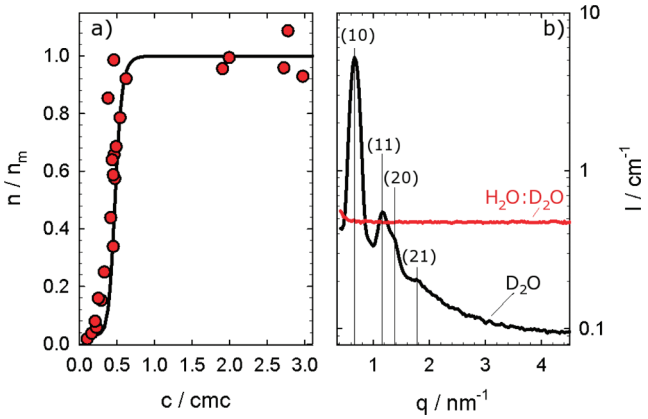

Figure 1. (a) Experimental adsorption isotherm of the surfactant $C_{12}E_5$ in SBA-15 plotted as relative loading $f = n/n_m$ vs relative concentration c/cmc. (b) SANS curves from SBA-15 immersed in D_2O and in the contrast-matching H_2O/D_2O mixture. The positions of the four leading Bragg reflections are indicated by vertical lines.

Scheme 1. (a) Sketch of the Mesopore Lattice of SBA-15; (b,c) Surface Aggregates of the Surfactant in the Cylindrical Pores in Top View (Axial Direction) and Side View (Parallel to the Pore Axis); (d) Radial Scattering Length Density Profile $\rho(r)$ Adopted in the Data Analysis

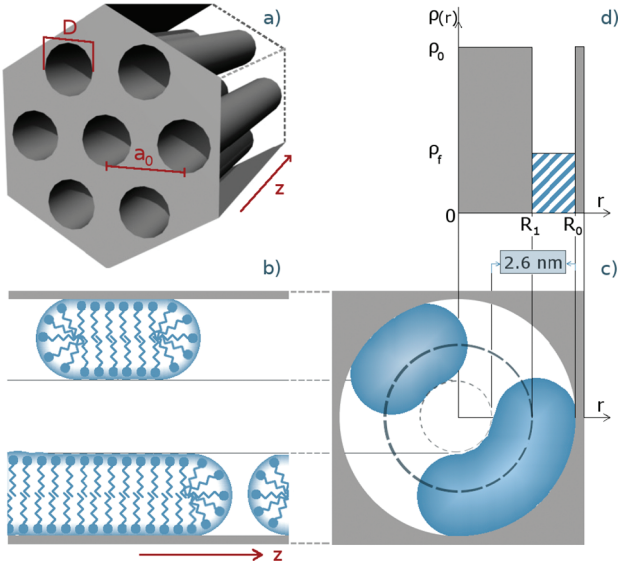

nanopores arranged side-by-side in a two-dimensional (2D) hexagonal lattice (space group *P6mm*),[14] as sketched in Scheme 1. X-ray diffraction profiles from our SBA-15 sample exhibit five well-resolved Bragg reflections from which we derive a lattice parameter a_0 of 10.2 nm and a pore diameter D = 8.1 nm, using the procedure described in ref 15, in agreement with the pore size determined by nitrogen adsorption on the basis of the Kruk−Jaroniec−Sayari (KJS) prescription.[16] The adsorption isotherm of $C_{12}E_5$ in this SBA-15 sample is shown in Figure 1a. It has a sigmoidal shape with a sharply rising section at a concentration c/cmc ≈ 0.4, where cmc = 6×10^{-5} M is the critical micelle concentration. This sharp increase in $n(c)$ is a signature of a phase transition of

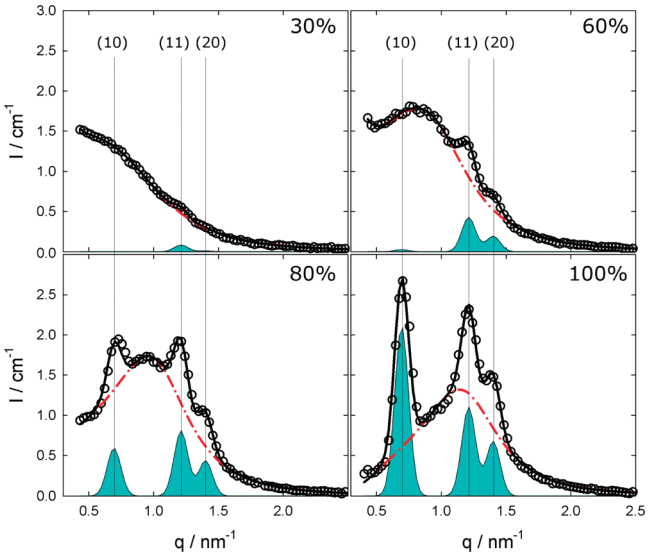

Figure 2. Scattering profiles $I(q)$ for SBA-15 with different surfactant loadings [(a) 30%; (b) 60%; (c) 80%; (d) 100%] in contrast-matching water (20 °C): scattering data (circles) and fit by the present model (full line), with the contribution by diffuse scattering (dashed-dotted red lines) and of the three leading Bragg peaks (blue areas). The positions of the Bragg reflections are marked by vertical lines.

the surfactant in the pore.[17] A limiting specific adsorption n_m = 1.25 mmol g^{-1} is reached shortly above the cmc. From the typical size of the SBA-15 particles (diameter 200 nm, length 2 μm), it is estimated that the ratio between inner and outer surface area is about 10, which means that ca. 10% of the surfactant was adsorbed at the outer surface of the particles and 90% in the cylindrical pores, corresponding to a maximum surfactant volume fraction $\varphi_m \approx 0.45$ in the pore space.

SANS measurements were made with a H_2O/D_2O solvent mixture of H_2O volume fraction 0.375, which has the same scattering length density as the silica matrix ($\rho = 3.7 \times 10^{10}$ cm^{-2}). When SBA-15 is immersed in this contrast-matching water, the Bragg reflections from the pore lattice are completely suppressed and only a constant background remains, mostly due to incoherent scattering from the protons of H_2O (Figure 1b).[18] Hence, in the presence of the surfactant ($\rho = 0.13 \times 10^{10}$ cm^{-2} for pure $C_{12}E_5$), scattering was due to the surfactant against a uniform background of matrix and water. Scattering profiles $I(q)$ of samples with surfactant filling factors $f = n/n_m$ corresponding to 30, 60, 80, and 100% of maximum loading are shown in Figure 2, where a constant scattering background (I_{bg} in eq 1) is already subtracted. All SANS profiles exhibit a broad diffuse-scattering peak superimposed with Bragg reflections, which are weak at low surfactant loadings but become prominent at high loadings. The positions of the Bragg reflections from the 2D hexagonal lattice at $q_{hk} = (4\pi/a_0\sqrt{3})(h^2 + k^2 + hk)^{1/2}$ (hk = 10, 11, 20) are indicated by vertical lines. To describe the SANS profiles quantitatively, we consider the total scattering amplitude as the sum of the individual contributions from all the mesopores (assuming that there is no correlation between the scattering

DOI: 10.1021/jz100279y | J. Phys. Chem. Lett. 2010, 1, 1442–1446

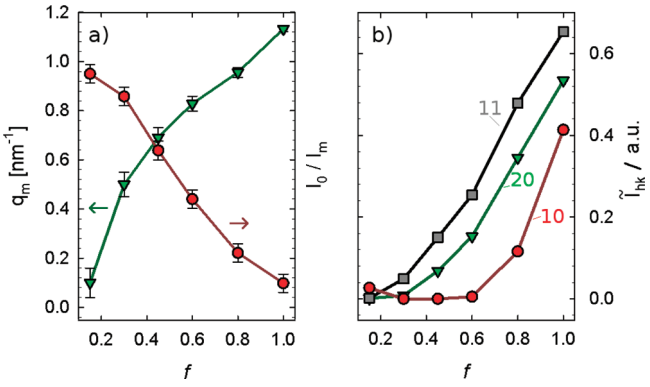

Figure 3. Primary results of data analysis as a function of the surfactant loading f: (a) position q_m and intensity ratio I_0/I_m of the correlation peak in the diffuse scattering; (b) integral intensities $\tilde{I}_{hk}$ of the leading Bragg reflections.

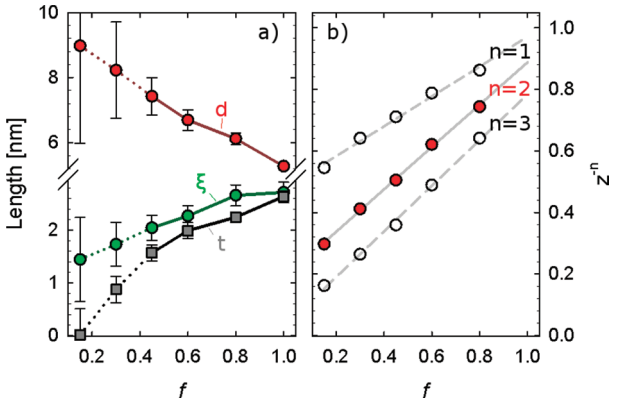

Figure 4. Length parameters that characterize the arrangement of surface aggregates of the surfactant in the pores as a function of the filling factor f: (a) interparticle distance of surfactant aggregates d, correlation length ξ, and layer thickness t; (b) scaling of the relative interparticle distance $z = d/d_{min}$ with the filling factor f (see text).

amplitudes in the different pores), which can be written in a compact way[19]

$$I(q) = I_{bg} + I_{diff}(q) + S(q)|F(q)|^2 \quad (1)$$

with $I_{diff} \propto (\pi/q)[\langle|A|^2\rangle - |\langle A\rangle|^2]$ and $F(q) = \langle A\rangle$, where $\langle A\rangle$ is the 2D scattering amplitude from a circular pore averaged spatially over all pores as well as circularly for a rotation around the pore axis. $\langle|A|^2\rangle$ is the analogous average of the amplitude squared, and the factor π/q is due to the spherical average of the cylindrical structures.

The last term in eq 1 is the Bragg diffraction and depends on the structure factor $S(q)$, which is the spherical average of the Bragg rods from the 2D pore lattice. $S(q)$ was modeled as a sum of three Gauss peaks centered at the respective positions q_{hk}. The widths of the Gauss peaks were obtained by data fitting, keeping them identical for all three peaks in a given diffraction diagram and for all surfactant loadings. The formation of a surfactant layer at the pore walls was modeled by a step-density profile $\rho(r)$ as indicated in Scheme 1d. This model is equivalent to the form factor of a cylindrical shell structure

$$F(q) = \frac{2\Delta\rho}{q(R_0^2 - R_1^2)}[R_0 J_1(qR_0) - R_1 J_1(qR_1)] \quad (2)$$

where $R_0 = D/2$ is the pore radius, R_1 is the inner radius of the surfactant layer, $\Delta\rho = \rho_0 - \rho_f$ is the density increment of the surfactant layer (mean scattering length density ρ_f) against matrix and water (ρ_0), and J_1 is the Bessel function of first order. The function $|F(q)|^2$ exhibits sharp minima, which move to larger q as the shell thickness $t = R_0 - R_1$ increases, causing a modulation of the intensities of the individual Bragg peaks with increasing t.[15]

The second term in eq 1 represents the diffuse scattering arising from surfactant aggregates in the silica matrix. We found that this can be represented by a scattering function for a disperse two-phase system with spatial correlations:

$$I_{diff}(q) = B(q)\frac{I_0}{(1 - I_0/I_m)(q^2/q_m^2 - 1)^2 + I_0/I_m} \quad (3)$$

where I_m and q_m represent the coordinates of the respective correlation peak. Equation 3 with $B = 1$ (when I_0 is the limiting value of I_{diff} at $q = 0$) was originally proposed for microemulsion systems by Teubner and Strey,[20] and similar expressions have been widely used to describe the time evolution of phase separating systems.[21,22] We use the previously proposed expression with $B(q) = q^4/(k + q^4)$, where k is a constant.[21] However, since this expression describes a bulk system rather than a fluid confined to cylindrical pores, eq 3 can only be considered a rough approximation. Nevertheless, we believe it captures the essence of the fluid inhomogeneities within the pores.

Analysis of the experimental scattering profiles in terms of eqs 1−3 is shown in Figure 2. It yields the parameters q_m and I_0/I_m of eq 3 and the integrated intensities $\tilde{I}_B(q_{hk}) = \int I_B(q_{hk})q^2 dq$ of the leading Bragg reflections. It is found that the position of the peak maximum (q_m) in $I_{diff}(q)$ moves to higher q, and the peak intensity parameter (I_0/I_m) decreases as the surfactant loading increases (Figure 3a). The Bragg intensity $\tilde{I}_{10}$ exhibits a shallow minimum near $f = 0.3$ and is the smallest of the three Bragg peaks at $f > 0.15$ (Figure 3b). This is a signature of a shell structure, clearly indicating that the surfactant forms a layer at the pore wall rather than forming micelles in the core.

From the present analysis we derive three length parameters that characterize the self-assembly of the surfactant in the pores: the average thickness t of the surfactant layer, the characteristic (quasi-periodic) distance d between surfactant aggregates (equivalent to the domain size in microemulsion systems), and the correlation length ξ of this quasi-periodic arrangement of surface aggregates. The quantities d and ξ are calculated from the parameters I_0/I_m and q_m of eq 3.[20] The resulting dependency of the three length parameters on the surfactant filling factor f is shown in Figure 4a. We first turn to the observation that the distance d between surfactant aggregates decreases as f increases. The value at the lowest surfactant loading ($f = 0.15$), $d \approx 10$ nm, is close to the lattice constant a_0 of the pore lattice and corresponds to one surfactant aggregate per 10 nm along each pore. In this regime of low surfactant loadings we expect isolated surfactant aggregates. The observed decrease in d then implies that

DOI: 10.1021/jz100279y | J. Phys. Chem. Lett. 2010, 1, 1442–1446

the number of surfactant aggregates increases with f. If the mean aggregate size is independent of the amount of surfactant in the pores, the number of aggregates, N, will be directly proportional to the filling factor. In nonconfined three-dimensional (3D) systems, N scales with the aggregate distance as $N \propto d^{-3}$, and we expect $f \propto z^{-3}$, with $z = d/d_{min}$. However, if the system is confined to 2D or 1D, scaling as $f \propto z^{-n}$ with $n = 2$ or 1, respectively, is expected. The experimental data conform to a scaling with $n = 2$, for which the standard deviation is nearly a factor 2 lower than for the fits with $n = 3$ and $n = 1$ (Figure 4b), indicating a significant influence of the excluded volume on the arrangement of the surfactant aggregates in the SBA-15 matrix. The correlation length ξ of this quasi-periodic arrangement is quite small at low filling fractions but increases with f (Figure 4a), and the ratio ξ/d increases from 0.15 at $f = 0.15$ to about 0.5 at $f = 1$. Values of ξ/d in a range from 0.25 to 0.5 are reported for microemulsion systems in the bulk phase.[20]

To estimate the mean size of surfactant aggregates in the pores (volume V_{agg}) we calculate the number of aggregates per unit mass of silica as $N = v_{tot}/d^3$, where v_{tot} is the volume per unit mass of the SBA-15 matrix, given by $v_{tot} = [\tilde{\rho}_S(1 - 2\pi S^2/\sqrt{3})]^{-1}$, with $\tilde{\rho}_S$ being the mass density of silica and $S = R_0/a_0$. From the known number of aggregates and the overall volume v of surfactant per unit mass of silica ($v = n/\tilde{\rho}$, with $\tilde{\rho}$ being the mass density of the surfactant) we obtain $V_{agg} = v/N$. The resulting values correspond to spherical particles of radius $R_{agg} = 2.6 \pm 0.2$ nm, or oblate ellipsoids[7,12] of small semiaxis $c = 1.3$ nm (see below and Scheme 1c for justification), and large semiaxis $a = 3.7 \pm 0.3$ nm, without systematic size dependence with the filling factor. This picture of isolated surface micelles is plausible at low surfactant loadings but is probably unrealistic at high loadings, as discussed below.

The average thickness t of the adsorbed surfactant layer increases with f (Figure 4a), and a similar increase is found for the density increment $\Delta\rho$ (not shown). The reader is reminded that the values of t result from angular averaging of the inhomogeneous density distribution in the pore and replacement of the resulting radial density profile $\rho(r)$ by a step profile. Due to this averaging, t will be smaller than the width of the surface aggregates as long as only part of the pore wall is covered by surfactant. Accordingly, surface micelles of some flattened geometry (such as the oblate ellipsoids mentioned above) and having a width of up to 3 nm are compatible with the observed layer thickness t at intermediate loadings. At the highest loading the mean film thickness reaches 2.6 nm. From the amount adsorbed and the volume of a hydrated surfactant molecule (0.97 nm^3)[9] we estimate that about 75% of the layer volume is occupied by surfactant at maximum loading, which suggests a morphology of interconnected bilayer patches. This picture is consistent with the pronounced increase in Bragg scattering intensity at high values of f seen in Figures 2 and 3b. Note, however, that the thickness of the surfactant layer at the pore walls remains much smaller than that of a bilayer at flat silica surfaces (4.2 nm for $C_{12}E_5$),[9] indicating a highly distorted structure of the layer.

In conclusion, by combining the information extracted from diffuse scattering and Bragg scattering, we find that the highly cooperative adsorption of the surfactant in the pores occurring at a bulk concentration $c \approx 0.4$ cmc involves the formation of isolated surfactant aggregates (surface micelles), increasing in number with the filling factor f, until they merge to interconnected patches at high surfactant loading. The observed scaling of the relative interaggregate distance $z = d/d_{min}$ with the surfactant filling factor ($f \propto z^{-2}$) indicates that the quasi-periodic arrangement of the surfactant aggregates in the SBA-15 particles is significantly affected by the excluded volume of the silica matrix. Further work on the self-assembly of different surfactants in the pores of SBA-15 is in progress.

METHODS

The adsorption isotherm of $C_{12}E_5$ in the SBA-15 sample was determined by equilibrating the silica powder with solutions containing appropriate amounts of the surfactant, and determining its concentration in the supernatant by surface tension measurements.[11] SBA-15 samples with surfactant filling factors f from 0.15 to 1 in contrast-matching H_2O/D_2O were prepared and transferred to specially designed slurry cells.[18] SANS measurements were performed at the small momentum transfer diffractometer D16 at Institut Laue-Langevin (ILL, Grenoble). The range of scattering vectors $q = (4\pi/\lambda)\sin(\theta)$ was $0.4 < q < 4.5$ nm^{-1}, with the scattering angle 2θ and the neutron wavelength $\lambda = 0.47$ nm ($\Delta\lambda/\lambda = 0.01$). Data acquisition times were between 2 and 3 h (total for two detector angles).

AUTHOR INFORMATION

Corresponding Author:

*To whom correspondence should be addressed. Tel.: +49 (0) 30 31424171. Fax: +49 (0) 30 31426602. E-mail address: findenegg@chem.tu-berlin.de.

ACKNOWLEDGMENT The authors wish to thank Jens Meissner for help with the determination of the surfactant adsorption isotherm in SBA-15. Neutron beam time at the Institut Laue-Langevin is also gratefully acknowledged. This work was supported by Deutsche Forschungsgemeinschaft (DFG) in the framework of SFB 448, Projects B1 and B14.

REFERENCES

(1) Nalaskowski, J.; Drelich, J.; Miller, J. D. Forces between Polyethylene Surfaces in Oxyethylene Dodecyl Ether Solutions as Influenced by the Number of Oxyethylene Groups. *Langmuir* **2008,** *24*, 1476–1483.

(2) Leermakers, F. A. M.; Koopal, L. K.; Lokar, W. J.; Ducker, W. A. Modeling of Confinement-Induced Phase Transitions for Surfactant Layers on Amphiphilic Surfaces. *Langmuir* **2005,** *21*, 11534–11545.

(3) Talens-Alesson, F. I.; Urbanski, R.; Szymanowski, J. Evolution of Resistance to Permeation during Micellar Enhanced Ultrafiltration. *Colloids Surf. A* **2001,** *178*, 71–77.

(4) Arai, N.; Yasuoka, K.; Zeng, X. C. Self-Assembly of Surfactants and Polymorphic Transitions in Nanotubes. *J. Am. Chem. Soc.* **2008,** *130*, 7916–7920.

DOI: 10.1021/jz100279y | *J. Phys. Chem. Lett.* **2010,** *1*, 1442–1446

(5) Schmuhl, R.; van der Berg, A.; Blank, D. H. A.; ten Elshof, J. E. Surfactant-Modulated Switching of Molecular Transport in Nanometer-Sized Pores of Molecular Gates. *Angew. Chem., Int. Ed.* **2006,** *45*, 3341–3345.
(6) Apel, P. Y.; Blonskaya, I. V.; Dmitriev, S. N.; Orelovitch, O. L.; Presz, A.; Sartowska, B. A. Fabrication of Nanopores in Polymer Foils with Surfactant-Controlled Longitudinal Profiles. *Nanotechnology* **2007,** *18*, 305302.
(7) Levitz, P. Aggregative Adsorption of Nonionic Surfactants onto Hydrophilic Solid/Water Interface. Relation with Bulk Micellization. *Langmuir* **1991,** *7*, 1595–1608.
(8) Grant, L. M.; Tiberg, F.; Ducker, W. A. Nanometer-Scale Organization of Ethylene Oxide Surfactants on Graphite, Hydrophilic Silica, and Hydrophobic Silica. *J. Phys. Chem. B* **1998,** *102*, 4288–4294.
(9) Böhmer, M. R.; Koopal, L. K.; Janssen, R.; Lee, E. M.; Thomas, R. K.; Rennie, A. R. Adsorption of Nonionic Surfactants on Hydrophilic Surfaces. An Experimental and Theoretical Study on Association in the Adsorbed Layer. *Langmuir* **1992,** *8*, 2228–2239.
(10) Steitz, R.; Müller-Buschbaum, P.; Schemmel, S.; Cubitt, R.; Findenegg, G. H. Lateral Structure of a Surfactant Adsorbed Layer at a Hydrophilic Solid/Liquid Interface. *Europhys. Lett.* **2004,** *67*, 962–968.
(11) Lugo, D.; Oberdisse, J.; Karg, M.; Schweins, R.; Findenegg, G. H. Surface Aggregate Structure of Nonionic Surfactants on Silica Nanoparticles. *Soft Matter* **2009,** *5*, 2928–2936.
(12) Giordano, F.; Denoyel, R.; Rouquerol, J. Influence of Porosity on the Adsorption of a Nonionic Surfactant on Silica. *Colloids Surf., A* **1993,** *71*, 293–298.
(13) Qiao, Y.; Schönhoff, M.; Findenegg, G. H. ^{2}H NMR Investigation of the Structure and Dynamics of the Nonionic Surfactant $C_{12}E_5$ Confined in Controlled Pore Glass. *Langmuir* **2003,** *19*, 6160–6167.
(14) Zhao, D. Y.; Feng, J. L.; Huo, Q. S.; Melosh, N.; Fredrickson, G. H.; Chmelka, B. F.; Stucky, G. D. Triblock Copolymer Synthesis of Mesoporous Silica with Periodic 50 to 300 Angstrom Pores. *Science* **1998,** *279*, 548–552.
(15) Jähnert, S.; Müter, D.; Prass, J.; Zickler, G. A.; Paris, O.; Findenegg, G. H. Pore Structure and Fluid Adsorption in Ordered Mesoporous Silica. I. Experimental Study by *in situ* Small-Angle X-Ray Scattering. *J. Phys. Chem. C* **2009,** *113*, 15201–15210.
(16) Jaroniec, M.; Solovyov, L. A. Improvement of the Kruk–Jaroniec–Sayari Method for Pore Size Analysis of Ordered Silicas with Cylindrical Mesopores. *Langmuir* **2006,** *22*, 6757–6760.
(17) Huinink, H. P.; de Keizer, A.; Leermakers, F. A. M.; Lyklema, J. Adsorption of Nonionic Surfactants in Hydrophilic Cylindrical Pores. A Thermodynamic Analysis. *Langmuir* **1997,** *13*, 6452–6460.
(18) Shin, T.; Findenegg, G. H.; Brandt, A. Surfactant Adsorption in Ordered Mesoporous Silica Studied by SANS. *Prog. Colloid Polym. Sci.* **2006,** *133*, 116–122.
(19) Guinier, A.; Fournet, G. *Small-Angle Scattering of X-Rays*; Wiley: New York, 1955.
(20) Teubner, M.; Strey, R. Origin of the Scattering Peak in Microemulsions. *J. Chem. Phys.* **1987,** *87*, 3195–3200.
(21) Fratzl, P.; Lebowitz, J. L.; Penrose, O.; Amar, J. Scaling Functions, Self-Similarity, and the Morphology of Phase-Separating Systems. *Phys. Rev. B* **1991,** *44*, 4794–4811.
(22) Binder, K.; Fratzl, P. Spinodal Decomposition. In *Materials Science and Technology: Phase Transformations in Materials*, 2nd ed.; Kostorz, G., Ed.; Wiley-VCH: Weinheim, Germany, 2001; Vol. 5.

DOI: 10.1021/jz100279y | *J. Phys. Chem. Lett.* **2010,** *1*, 1442–1446